MethodsX 13 (2024) 103039

Contents lists available at ScienceDirect

MethodsX

journal homepage: www.elsevier.com/locate/methodsx

A method to map land use impacts on microclimate regulation supply in urban environments

Paulo Pereira[a,*], Luis Valenca Pinto[a], Marius Kalinauskas[a], Egle Baltranaite[a], Eduardo Gomes[b,c], Miguel Inacio[a], Damia Barcelo[d]

[a] Environmental Management Laboratory, Mykolas Romeris University, Vilnius, Lithuania
[b] Centre for Geographical Studies, Institute of Geography and Spatial Planning, Universidade de Lisboa, Lisbon, Portugal
[c] Associated Laboratory TERRA, Portugal
[d] Department of Chemistry and Physics, University of Almería, Spain

ARTICLE INFO

Method name:
Microclimate regulation in urban environments

Keywords:
Land use
Land surface temperature
Microclimate regulation supply
Unmanned aerial vehicle
Urban areas

ABSTRACT

Land use impacts land surface temperature (LST), especially in urban areas where anthropogenic materials have a high capacity to store energy. Nevertheless, cities have many other land uses (e.g., forests, lawns) that can reduce LST and contribute to high microclimate regulation. In this work, we develop a method to map land use impacts on microclimate regulation supply using an Unmanned Aerial Vehicle (UAV). A detailed methodology was developed for 1) UAV's mission planning, 2) field data collection for method validation, 3) RGB and thermal mission reconstruction, 4) land use classification, 5) data extraction and 6) spatial and statistical analysis. The method developed can be beneficial to local authorities and transferable to other realms. It will allow us to understand the impacts of different land uses on microclimate regulation. For this, an area with heterogeneous land uses was used as a test site.

- A novel methodology was created to map land use impacts on microclimate regulation supply in urban areas;
- High-resolution UAV RGB and thermal imagery for land-use classification and surface temperature analysis;
- The method can help understand the capacity of the different land uses on microclimate regulation;

Specifications Table

Subject area:	Environmental Science
More specific subject area:	Ecosystem Services; Proximal Sensing
Name of your method:	Microclimate regulation in urban environments
Name and reference of original method:	Not applicable
Resource availability:	DJI Mavic Enterprise 3M DJI Mavic Enterprise 3T MESTEK Digital Infrared Thermometer Pyrometer Laser with K-Probe

(*continued on next page*)

* Corresponding author.
E-mail address: pereiraub@gmail.com (P. Pereira).

https://doi.org/10.1016/j.mex.2024.103039
Received 11 September 2024; Accepted 6 November 2024
Available online 9 November 2024

Computer	Intel(R) Core (TM) i9-10900X CPU @ 3.70GHz 3.70 GHz and 64.0 GB Memory
Google Earth	N
DJI Terra	Software
ArcGIS Pro	(ver. 3.1.2)
JASP	0.18.3.0
Online Plotly	(https://chart-studio.plotly.com/)

Background

Land use changes are one of the most critical drivers of environmental change [1]. It is also well known that urban expansion is one of the leading causes of land degradation, biodiversity loss and climate change [2–4]. Another effect of urbanisation is the increase in temperature due to substituting vegetation cover with concrete or other materials of anthropogenic origin, such as asphalt [5], with negative implications on microclimate regulation. Microclimate regulation by the ecosystems is understood as their capacity to moderate the temperature and other weather variables (e.g., humidity) at the local level [6], such as urban areas. The higher temperature in cities compared to their surroundings (e.g., forests, agricultural areas) is known as the urban heat island effect [7], and it is severe in highly dense urban areas. This urban effect on the temperature can amplify the effects of climate change in the cities, mainly during heat wave episodes that are becoming more frequent and severe. Between 2000–2019, heat waves in urban areas were responsible for 489 000 deaths each year,[1] globally. Although land use in urban areas mainly comprises buildings, urban green and blue areas (UGBI) (e.g., urban forests, parks, lakes) are essential components that regulate the microclimate. Several studies highlight the importance of UGBI to microclimate regulation [e.g., 8,9].

Remote sensing data contributed importantly to mapping and identifying the impacts of the different surfaces (fabric/non-fabric) on the temperature in urban areas [10]. More recently, unmanned aerial vehicles (UAVs) have been applied to conduct high-resolution studies, which is critical to better understanding the temperature small-scale variation [11]. UAVs present many advantages compared to satellite data since data can be collected anytime without cloud cover restrictions. This is especially important in areas with a high cloud coverage for most of the year (e.g., temperate, boreal, and tropical biomes). However, some disadvantages exist compared to satellite data, such as the limitations regarding the meteorological conditions (e.g., strong wind and precipitation), the need to pre-process and manage the data, small-scale analysis, and the legislation restrictions (e.g., no-fly zones) [12]. Several works were conducted to assess land surface temperature (LST) in urban areas using UAVs [e.g., 13–16]. LST has been used as an indicator to assess microclimate regulation ecosystem services (ES) (CICES v5.1: 2.3.6.2 - Regulation of temperature and humidity, including ventilation and transpiration at local scales) [17–19]. Nevertheless, a comprehensive methodology to map and assess microclimate regulation ES using UAV thermal analysis, considering data collection in the field, land use classification, and statistical and spatial analysis, is lacking. This is essential to assess microclimate regulation in urban areas and guide future studies using UAVs. Thus, this work aims to provide a compressive methodological framework to assess the supply of microclimate regulation in urban areas using UAVs.

Method details

UAV mission planning and image reconstructions

The method was tested in Vilnius, Lithuania. The study area has 108 ha, and the land use is diverse (e.g., grasslands, scrublands, buildings, trees, and forests (Fig. 1). Six missions were conducted in July 2024 (Table 1) during a heat wave period that affected different regions of Europe.[2] The weather conditions observed during the flight time are shown in Table 1. The missions were conducted using two drones: DJI Mavic Enterprise 3M (hereafter DJI 3M), equipped with a multispectral and RGB camera, and DJI Mavic Enterprise 3T (hereafter DJI 3T), equipped with a thermal camera. The characteristics of both drones are shown in Table S1. Before establishing the missions, a framework was developed to implement the methodology (Fig. 2). Previously, to go to the field, a Keyhole Markup Language (KML) of the area of interest was created using Google Earth Online.[3] Once the study area was selected, the KML was uploaded in the DJI Pilot 2 software[4] (available in both drones remote control) to create a flight mission in DJI Mavic Enterprise 3M and 3T (Fig. S1). The flight duration of DJI 3M was 1 h 2 m 42 s, and DJI 3T was 2 h 6 m 11 s. The missions were executed each day at around 12:00 am, more precisely between 11:50 and 14:10, when the sun reaches the zenith in the northern hemisphere summertime. This was important to minimise the impact of building and tree shadows on LST. DJI 3M had a ground sample distance of 5.01 cm and DJI 3T of 10 cm. DJI 3M flew at an altitude of 108.4 m and DJI 3T at 75.8 m. In both UAVs, the safe take-off altitude was 20 m, the flight speed was 8 m/s, the side overlapping ratio was 70%, the front overlap ratio was 80%, and the margins were 10 m (Table 2). In each mission, the DJI Mavic 3M took 1550 photos, and the DJI 3T took 5290 photos. The images were saved in a micro-SD card inserted in the UAVs and later extracted and processed.

[1] https://www.who.int/news-room/fact-sheets/detail/climate-change-heat-and-health.
[2] https://www.theguardian.com/world/article/2024/jul/19/europe-heatwave-greece-italy-croatia-health-warnings.
[3] https://earth.google.com/.
[4] https://www.dji.com/lt/downloads/djiapp/dji-pilot.

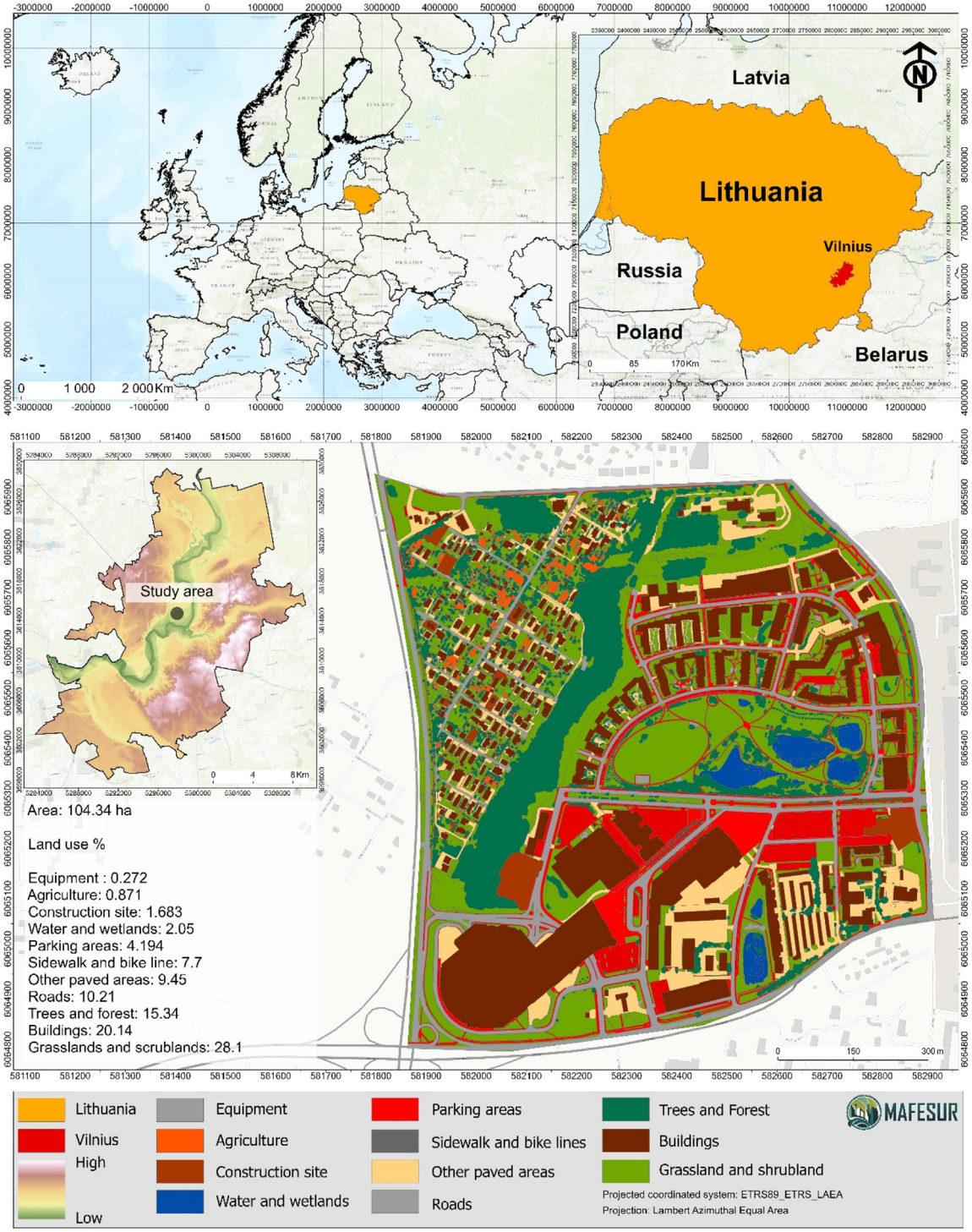

Fig. 1. Study area.

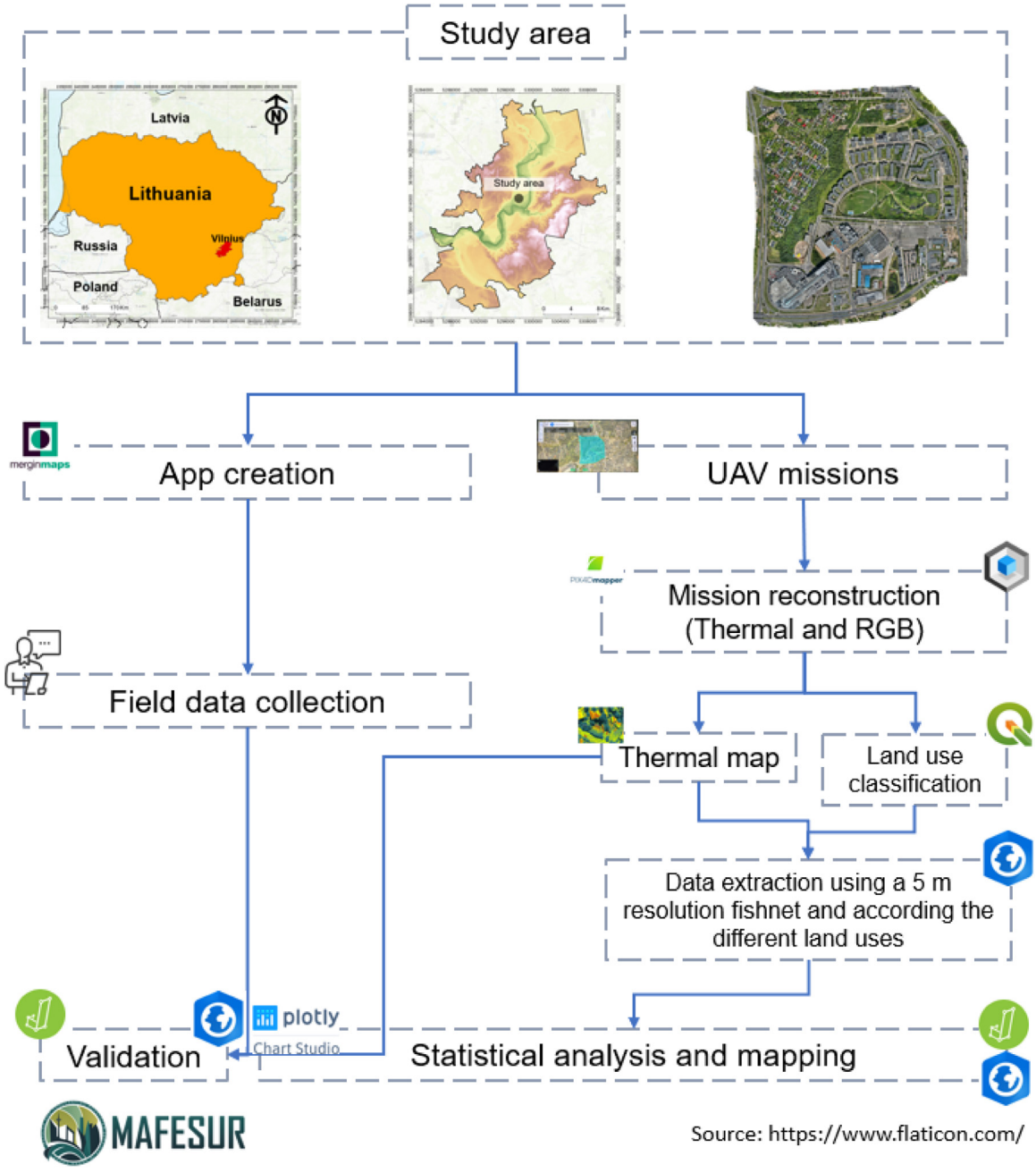

Fig. 2. Methodological framework applied.

Table 1
Meteorological conditions during the flight.

Day	Weather	Air temperature (°C)	Relative Humidity (%)
2024-07-10	Sunny	32.0	33.8
2024-07-11	Sunny	35.3	32.4
2024-07-14	Cloudy	27.4	52.1
2024-07-16	Sunny	31.2	43.9
2024-07-18	Partly cloudy	27.8	45.5
2024-07-19	Partly cloudy	24.8	43.8

Table 2
UAV missions' information.

	DJI 3M	DJI 3T
Mapping area	1.08 km^2	1.08 km^2
Flight time	1 h 2 m 42 s	2 h 6 m 11 s
Ground sample distance	5.01 cm	10 cm
Altitude	108.4 m	75.8 m
Safe take off altitude	20 m	20 m
Speed	8 m/s	8 m/s
Slide overlap ratio	70%	70%
Frontal overlap ratio	80%	80%
Margin	10 m	10 m

DJI 3M data was processed in DJI Terra[5] software for generating an RGB mosaic. DJI Terra employs advanced algorithms for processing aerial imagery, allowing the production of 2D and 3D models. To generate an RGB 2D model (mosaic), several steps were followed: (1) select "New Mission" and choose the mission type "Visual Light"; (2) define the mission's name; (3) in the section "Photos" choose a single or multiple folder of the drone mission. The acquired images have embedded positional data (POS), which includes GPS coordinates and camera orientation at the time of capture. In this step, DJI Terra software lays out the point location of the photos on a map. The photo's POS information can be visualised in the software, exported or downloaded. The software also identifies camera parameters, and since the photos were captured using a DJI proprietary drone, it identifies the DJI 3M camera parameters; (4) in the section "Aerotriangulation", the setting "Scene" was defined as "Normal", and the "Computational Method" to "Standalone Computation". In the "Advanced" settings, the "Feature Point Density" was set to "High" and the "Distance to Ground/Subjects" was set to 100 meters; (5) we selected "2D Map" and defined the "Scene" as "Mapping Scenarios", the "Computational Method" to "Standalone Computation", and the "Resolution" to "High". In the "Advanced" settings the "Output Coordinate System", specifically the "Horizontal Datum Settings" was set to "WGS 84 / UTM Zone 35N" and the "Geoid Settings" as "Default"; (6) the last step is to "Start the Reconstruction", which will generate an RGB mosaic file as a "GeoTIFF" file along with other files (e.g., POS information, Reconstruction Report). The positional accuracy, based on the output report, of the final mosaics is described in Table S2.

DJI 3T data was processed in Pix4DMapper[6] software for generating an LST mosaic. Pix4DMapper is a photogrammetry software that converts aerial drone images into highly precise 2D maps and 3D models, including generating thermal mosaics. To generate a thermal 2D mosaic, Pix4DMapper requires images to be in "TIFF" format. However, the images captured by the DJI 3T are outputted as "JPEG". Therefore, prior to processing the imagery data in Pix4DMapper it is necessary to do an intermediate step: to convert "JPEG" to "TIFF" using the DJI Image Processor.[7] This tool enables the extraction of temperature data in Celsius from DJI thermal imagery. To convert the images in DJI Image Processor (1) choose the "DJI Thermal Converter"; (2) click on "Choose Images Folder"; (3) define the flight height in meters, in the box "Distance"; define the average humidity (acquired based on the collected data), in the box "Humidity"; (4) "Emissivity" and "Reflectance" were set as "Default"; (5) click on "Start Batching Processing". After the images were converted to "TIFF," it was possible to generate a thermal 2D mosaic using Pix4DMapper.

The process follows several steps: (1) select "New Project" and define the project name, the output folder location, and the "Project Type" as "New Project"; (2) in the section "Select Images", choose "Select Directory" (the TIFF file directory. At this point, the images are added to the software. Select "Next", and the software will start to read the EXIF information in each image added; (3) in the "Image Properties" section the "Coordinate System" was set to "Datum: WGS 1984; Coordinate System: WGS84 (EGM 96 Geoid)", the "Geolocation Accuracy" was set to "Standard", and the software detected automatically the camera model "M3T_9.1_640 × 512 (Greyscale)". At this point click "Next"; (4) in the section "Processing Options Template" choose the "Thermal Camera" and click "Finish"; (5) select "Processing Options"; (6) in the section "1. Initial Processing" in the tab "General" for the "Keypoints Image Scale" we selected "Fill" and for the "Quality Report," we selected "Generate Orthomosaic Preview in Quality Report". In the tab "Matching" for the "Matching Image Pairs" we selected "Aerial Grid or Corridor". In the tab "Calibration" for the "Targeted Number of Keypoints" we selected "Automatic", for the "Calibration" we selected "Calibration Method: Alternative", "Internal Parameters Optimisation: All" and "External Parameters Optimisation: All". For "Rematch" we selected "Automatic". In the section "2. Point Cloud and Mesh" in the tab "Point Cloud", for the "Point Cloud Densification" we selected "Image Scale: 1 (Original image size, Slow); Multiscale", "Point Density: High (Slow)" and "Minimum Number of Matches: 3". In the tab 3D Texture Mesh, we selected "Generate 3D Texture Mesh" and "Settings: High Resolution". 3D Mesh was exported as FBX file. In the tab "Advanced", for the "Point Cloud Densification" we selected "Matching Window Size: 7×7 pixels", for "Image Groups" (Point Cloud, Mesh Geometry and Mesh Texture) we selected "Greyscale". For "Point Cloud Filters" we selected "Use Processing Area" and "Use Annotations". Finally, for "3D Texture Mesh Settings", "Sample Density Divider" was set to 1. In the section "3. DSM, Orthomosaic and Index", in the tab "DSM and Orthomosaic", "Resolution" was set to "Automatic: 1 x GSD". For the "DSM Filters" we selected "Use Noise Filtering" and "Use Surface Smoothing: Sharp". In the tab "Index Calculator" for "Radiometric Processing and Calibration" we selected "Correction Type: Camera

[5] https://enterprise.dji.com/dji-terra.
[6] https://www.pix4d.com/product/pix4dmapper-photogrammetry-software/.
[7] https://github.com/MiroRavaProj/DJI-Tools-and-Stuff.

Only". For "Resolution" we selected "Automatic: 1x GSD" and "Downsampling Method: Gaussian Average". For "Reflectance Map" we selected "GeoTIFF" and "Merge Tiles". For "Indices" we selected "greyscale = greyscale". In the section "Resources and Notifications" for the "Maximum Resources Available for Processing" we selected "RAM [GB]: 64" (the maximum available) and "CPU Threads: 20" (the maximum available). For "NVIDIA CUDA Capable Devices" we selected "GPU Device 1: NVIDIA RTX A5000"; (7) select "Ok"; and finally (8) select "Start Processing". Based on the output report, the positional accuracy of the final mosaics is described in Table S3.

The processing of both RGB and LST mosaics was done using a desktop computer equipped with an Intel(R) Core (TM) i9-10900X CPU @ 3.70 GHz [20] (hardware specifications in Table S4). The RGB reconstruction took approximately 2 hours, and LST 16 hours.

App creation and data collection

To collect field data in different aggregated land uses (lawns, forest and urban), an app was created using the Mergin Maps mobile app and associated services[8] (Fig. 2). The app allows for simple and efficient integration with QGIS projects through a plugin, ensuring data synchronisation between multiple field users and the main project in the Mergin Maps server. The Mergin Maps project was prepared in QGIS. First, a set of survey points was defined according to the study area and added to a Geopackage (.gpkg) file. Here, several fields were created to add ground surface temperature data. The data collection form was set and optimised in QGIS through the QGIS form designer. The legend of the survey points layer was configured to easily visualise the data collection status for each location ('no data collected', 'data partially collected', and 'all data collected'). Background layers were added to the project to ensure easier navigation in the field. Ten measurement points were distributed across the studied area in different aggregated land use types (lawns, forest and urban) in accessible areas (Fig. S2). Data was collected by two teams simultaneously with the UAV's missions. For this work, 30 ground surface temperatures were measured per mission using a MESTEK Digital Infrared Thermometer Pyrometer Laser with K-Probe. The device specificities are shown in Table S5. One hundred eighty measurements were taken during the 6 missions (60 per land use).

Land use classification

Land use classification was conducted using the RGB image from the July 10th mission (DJI 3M) at a resolution of 5.01 cm using QGIS (v3.34.8 LTR),[9] via manual digitalisation. Initially, we considered an automated classification through object-based analysis[10] in Google Earth Engine (GEE). However, several issues emerged, such as cars, and roof complex structures (e.g., ventilation systems). Also, the study area size and the high image resolution analysis resulted in out-of-memory errors in GEE. Therefore, we opted for a manual classification, which took approximately 2/3 weeks. The resulting land use classes are shown in Fig. 1. They include equipment (e.g., basketball playgrounds), agriculture (e.g., urban gardens), parking areas, sidewalks and bike lanes, other paved areas (e.g., gas stations, paved areas in private houses), roads, trees and forest, and grasslands and scrublands.

Data extraction and statistical analysis

To extract LST temperature from the resulting thermal map (raster layer), a fishnet point layer (5 m resolution) was created using the ArcGIS Pro fishnet tool.[11] We used a fishnet with a 5 m resolution because the computer (Table S4) did not have enough power to process data at a highresolution, such as 5 or 10 cm. Therefore, more computer power is needed to process data for large areas at a very high resolution. Using this fishnet, data was collected from the LST raster layer using the ArcGIS Pro extract multivalues to points tool.[12] Subsequently, the shapefile was exported as a dbf file and converted to a CSV file for statistical analysis in JASP. 0.18.3[13] (Fig. 2). The same procedure was applied to the ground data points used for validation from the 6 missions conducted. LST validation was carried out using a linear regression that considered all the samples, specific land uses, and weather types. The validation quality was assessed using R2, root mean square error (RMSE), standardised residuals, and Q-Q plot. Graphics were elaborated using online Plotly.[14] A Kruskal-Wallis ANOVA test was conducted in JASP to assess the statistical differences among land uses. If significant differences were found, a Dunn's post-hoc test was applied.

Method results, validation and limitations

Considering all the land uses and weather types, the validation shows an R^2 of 0.751 and an RMSE of 4.593°C. Overall, UAV LST data overestimated the temperature (Fig. 5). The R^2 was low when the regressions were conducted according to the aggregated land uses. The lawn's highest values were identified, and the forest's lowest. In all the cases, the RMSE was lower than the observed in the model that considered all the variables (Table 3). Regarding the weather conditions, the R^2 values were similar to those identified in

[8] https://merginmaps.com/.
[9] https://qgis.org/download/.
[10] https://developers.google.com/earth-engine/guides/image_objects.
[11] https://pro.arcgis.com/en/pro-app/latest/tool-reference/data-management/create-fishnet.htm.
[12] https://pro.arcgis.com/en/pro-app/latest/tool-reference/spatial-analyst/extract-multi-values-to-points.htm.
[13] https://jasp-stats.org/.
[14] https://chart-studio.plotly.com/.

Table 3
Regression results according to the different validation points in the different land uses (*N*=180).

Land use	R	R^2	Adjusted R^2	RMSE (°C)
Lawn	0.68 (p<0.001)	0.45	0.44	4.206
Forest	0.59 (p<0.001)	0.34	0.33	1.754
Urban	0.63 (p<0.001)	0.40	0.39	3.596

Table 4
Regression results according to the different validation points in the different weather conditions (*N*=180).

Land use	R	R^2	Adjusted R^2	RMSE (°C)
Sunny (*N*=90)	0.85 (p<0.001)	0.72	0.72	5.104
Partially cloudy (*N*=60)	0.86 (p<0.001)	0.76	0.76	3.958
Cloudy (*N*=30)	0.89 (p<0.001)	0.84	0.83	2.859

the model, considering all the variables. The highest value was identified in cloudy conditions, and the lowest was in sunny conditions. The RMSE observed in sunny conditions was higher than the identified in the other weather conditions (Table 4). It was also higher than the observed in the model considering all the variables. In all the regressions, considering all the samples, aggregated land uses and weather conditions, the standardised residuals followed the normal distribution, and the Q-Q plots were linear and close to the 1:1 line (Figs. 3; S3 and S4). This shows that the results obtained in the different models were valid. Overall, the validation results are good and acceptable when considering all the samples and the weather conditions (R^2>0.70). The results, according to the aggregated land uses, were low, especially in forest land use, and this is due to the difference between the temperatures observed above the tree canopy by the UAV and the ground surface below the canopy. Canopy shadows decrease ground temperature [e.g., 21]. For instance, previous works suggested that shadowed areas could be classified as separate units using machine or deep learning techniques [e.g., 22,23]. This could be considered in future works as well. In sunny conditions, the regrx3ession value was lower, and this can be attributed to the shadow effect of the trees and buildings, even though we tried to minimise this impact by conducting the missions near 12:00 am. This can be attributed to trees and building shadows that reduce the relation between UAV LST and ground-measured temperatures. Urban morphology and roughness affect temperature [e.g., 24,25]. The RMSE identified was especially high (5.104°C) in sunny conditions, attributed to the abovementioned factors. Similar or high RMSEs between LST were measured in previous works [e.g., 26,27]. To illustrate the results, we used data from one of the flights (2024-07-10). The microclimate regulation was significantly lower in building areas (high LST) than in all the other land uses. Better conditions for microclimate regulation (low LST) were supplied by water and wetlands, trees and forests and agriculture areas (Fig. 4). The spatial distribution of microclimate regulation for 2024-07-10 supports the claim above (Fig. 5). It is worth saying that the very low LST observed was attributed to cooling systems installed on buildings' roofs and the high temperatures LST was attributed to the black rooftops.

Although the method is robust, several limitations need to be highlighted. For instance, 1) flight time per UAV battery is limited to approximately 37-43 minutes, depending on the wind speed conditions (Table S1). Therefore, the UAV needs to return several times to change batteries. This increases the flight time, especially in missions that cover large areas [20]; 2) UAV microclimate regulation supply assessment is limited to small areas since there are restrictions regarding the distance between the remote control and the UAVs; 3) in cities, flight restrictions may apply (e.g., military or security areas, airports), limiting the study area extension; 4) buildings are often an obstacle to the communication between the pilot and the drone; 5) the time to measure LST using a UAV is limited and cannot be extended since the weather conditions (e.g., sun position and energy, cloud cover) and their effect on surface temperature can change fast during the day; 6) surface litter may also affect temperature reflectance. For instance, in Figs. 3 and 5, we observed that some values observed are negative in different land uses. For instance, in buildings, this can be attributed to different insulation materials, such as polyethene foam and phenolic foam, or air conditioning or refrigeration systems. The temperature sensor is measuring the thermal radiation temperature emitted by these insulation materials or air conditioning or refrigeration systems [e.g., 11]. Regarding land uses (e.g., construction sites, grassland and shrubland, parking areas, other paved areas, sidewalks and bike lanes), this can be attributed to litter on the soil surface. For instance, previous works observed that microplastics (e.g., plastic bottles) can reflect negative temperatures [28]. Nevertheless, the effects of litter on thermal reflectance need further studies; 7) the limited time to measure ground temperature that needs to be conducted simultaneously with the UAV mission. This requires more than one team to complete the work in time, especially if the study area is large and of difficult accessibility. This was the reason why, in this study, ground measures were taken in aggregated land use classes; 8) inaccessibly to some parts of the study area because it was private and fenced property (e.g., urban gardens); and 9) the very high-spatial resolution data acquisition (5 cm for land use classification and 10 cm for LST analysis) generates very large datasets and processing this data can take several hours, even we used a powerful computer (Table S4). The images' high resolution limited the application of an object-based analysis classification. This was also true when we conducted the statistical analysis using data at 10 cm resolution.

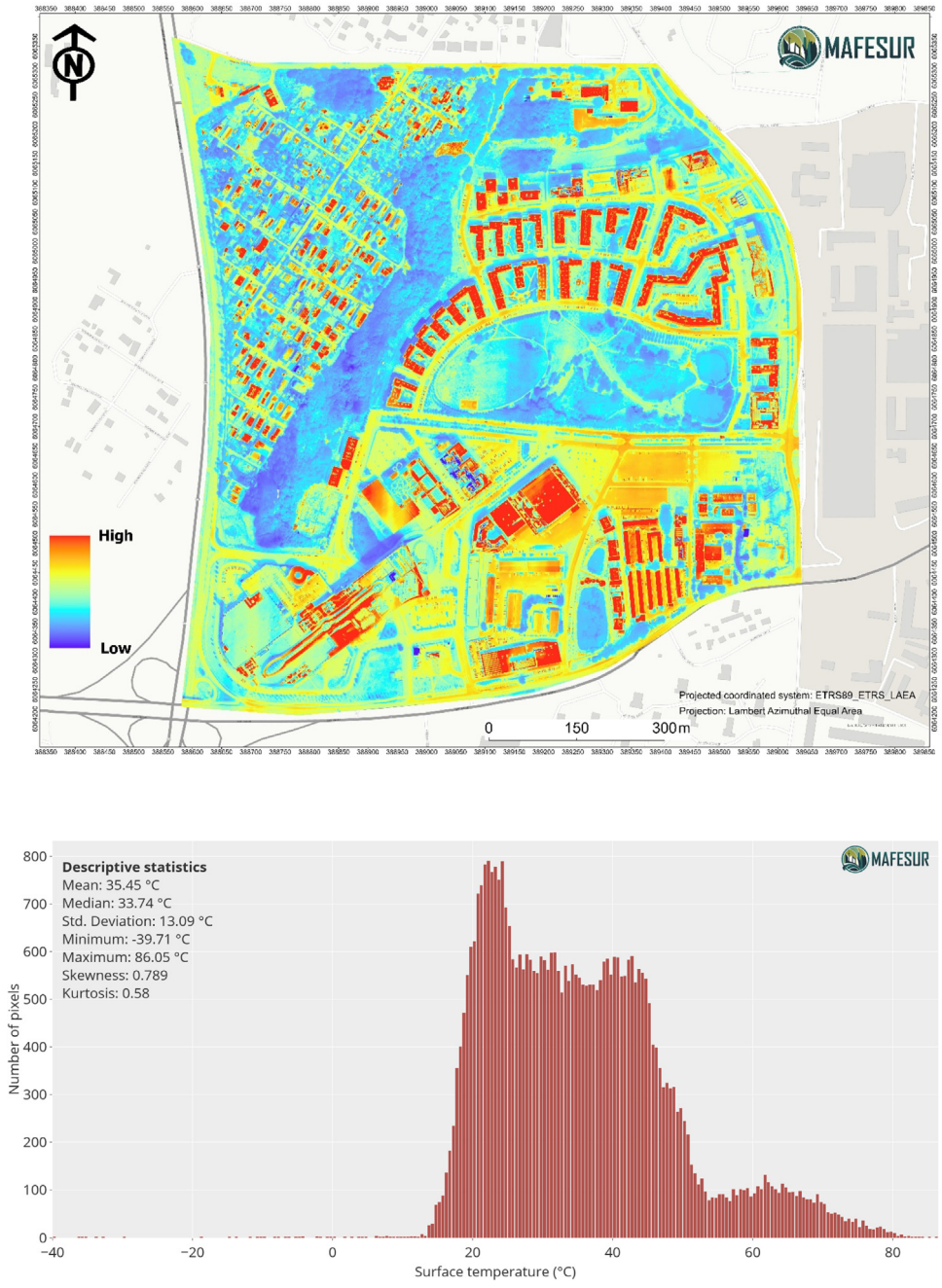

Fig. 3. Example of the surface temperature obtained for 2024-07-10 and the respective histogram.

In this work, we developed a robust method to assess the supply of microclimate regulation in urban areas that can be transferred to other cities. We only showed data from the summer season. Nevertheless, the method can be applied in different seasons and weather conditions. Increasing the number of points measured is essential to make the work more robust. However, more human resources are needed to increase the ground cover points for each mission. This is especially relevant in large areas. Finally, the results obtained with this method can be relevant for local authorities to understand the impact of the different surfaces on microclimate regulation supply under different weather conditions and seasons. This will help in designing future strategies and establishing nature-based solutions (e.g., green roofs, cool pavements) to reduce the urban heat island [29] and the impacts of climate change-related events such as heat waves that are especially relevant in urban areas [30].

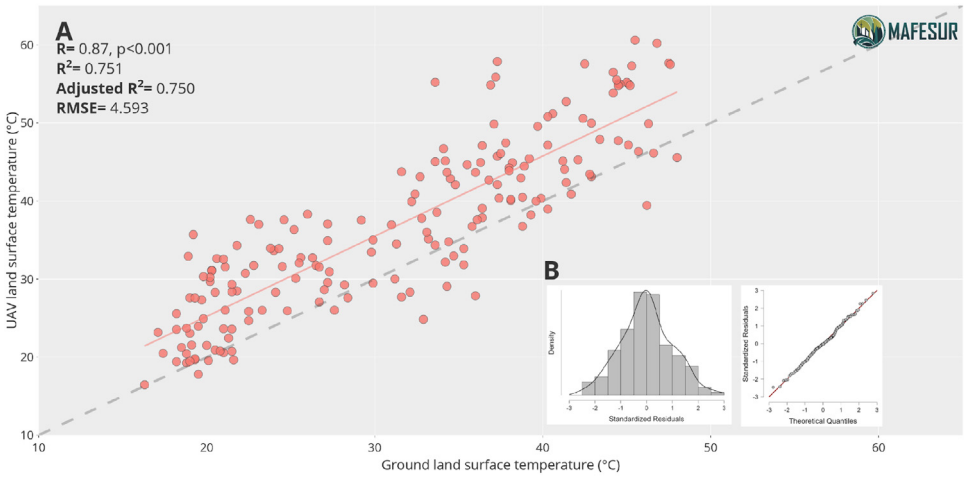

Fig. 4. A) Regression model between UAV and ground surface temperature and B) standardized residuals and Q-Q plot. Red line (linear regression) and grey dotted line (1:1 line).

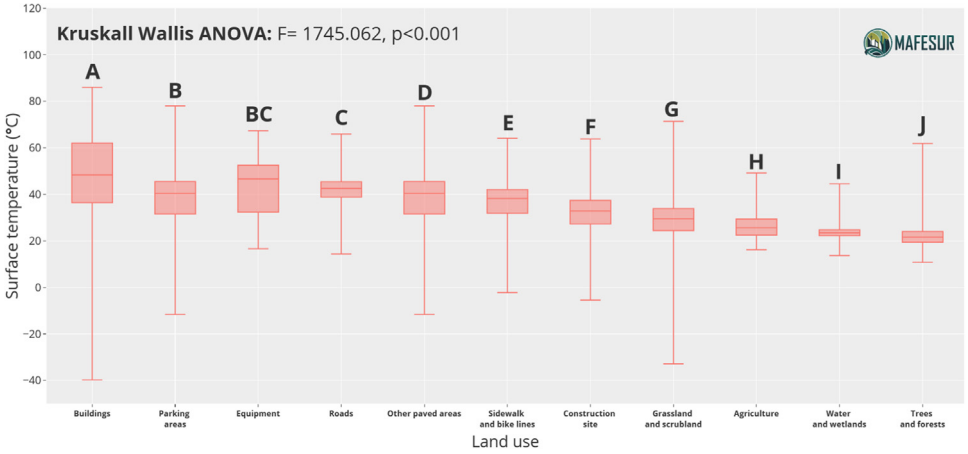

Fig. 5. Microclimate regulation supply according to the different land uses. Different letters above the box-whiskers show significant differences within land uses at a $p<0.05$.

CRediT author statement

Paulo Pereira: Conceptualization; Methodology; Investigation; Formal analysis; Investigation; Resources; Data Curation; Writing - original draft; Project administration, **Luis Valenca Pinto:** Methodology; Visualization; Writing - review & editing, **Marius Kalinauskas:** Methodology; Investigation; Visualization; Writing - review & editing, **Egle Baltranaite:** Investigation, Writing - review & editing, **Eduardo Gomes:** Investigation, Writing - review & editing, **Miguel Inacio:** Methodology; Investigation; Resources; Writing - review & editing, **Damia Barcelo:** Writing - review & editing.

Ethics statements

The work did not involve human beings.
The work did not involve animals.
The work did not involve data collected from social media platforms.

Declaration of competing interest

The authors declare that they have no known competing financial interests or personal relationships that could have appeared to influence the work reported in this paper.

Data availability

Data will be made available on request.

Acknowledgments

The work is supported by the project MApping and Forecasting Ecosystem Services in URban areas (MAFESUR), funded by the Lithuanian Research Council (Contract: Nr. P-MIP-23-426).

Supplementary materials

Supplementary material associated with this article can be found, in the online version, at doi:10.1016/j.mex.2024.103039.

References

[1] E. Gomes, M. Inacio, K. Bogdzevic, M. Kalinauskas, D. Karnauskaite, P. Pereira, Future land-use changes and its impacts on terrestrial ecosystem services: a review, Sci. Total Environ. 781 (2021) 146716, doi:10.1016/j.scitotenv.2021.146716.
[2] Y. Yang, Y. Nan, Z. Liu, D. Zhang, Y. Sun, Direct and indirect losses of natural habitat caused by future urban expansion in the transnational area of Changbai Mountain, Sustain. Cities Soc. 63 (2020) 102487, doi:10.1016/j.scs.2020.102487.
[3] Z. Ren, Y. Fu, Y. Dong, P. Zhang, X. He, Rapid urbanisation and climate change significantly contribute to worsening urban human thermal comfort: a national 183-city, 26-year study in China, Urban Clim. 43 (2022) 101154, doi:10.1016/j.uclim.2022.101154.
[4] R.A.C. Torres, J. Wang, J. Zhang, L. Liu, Y. Lan, Temporal analysis of land degradation and urban expansion in central Yunnan Province using remote sensing for supporting sustainable development goals 11/15, Ecol. Indic. 163 (2024) 112058, doi:10.1016/j.ecolind.2024.112058.
[5] M. Shamsaei, A. Carter, M. Vaillancourt, A review on the heat transfer in asphalt pavements and urban heat island mitigation methods, Constr. Build. Mater. 359 (2022) 129350, doi:10.1016/j.conbuildmat.2022.129350.
[6] Y. Wang, F. Bakker, R. de Groot, H. Wörtche, Effect of ecosystem services provided by urban green infrastructure on indoor environment: a literature review, Build. Environ. 77 (2014) 88–100, doi:10.1016/j.buildenv.2014.03.021.
[7] S.W. Kim, R.D. Brown, Urban heat island (UHI) intensity and magnitude estimations: a systematic literature review, Sci. Total Environ. 779 (2021) 146389, doi:10.1016/j.scitotenv.2021.146389.
[8] S. Erlwein, T. Zolch, S. Pauleit, Regulating the microclimate with urban green in densifiying cities: joint assessment on two scales, Build. Environ. 205 (2021) 108233, doi:10.1016/j.buildenv.2021.108233.
[9] S. Arzberger, M. Egerer, M. Suda, P. Annighöfer, Thermal regulation potential of urban green spaces in a changing climate: winter insights, Urban For. Urban Green. 100 (2024) 128488, doi:10.1016/j.ufug.2024.128488.
[10] J. Hofierka, M. Gallay, K. Onačillová, J. Hofierka Jr, Physically-based land surface temperature modeling in urban areas using a 3-D city model and multispectral satellite data, Urban Climate 31 (2020) 100566, doi:10.1016/j.uclim.2019.100566.
[11] Ahmad, J.A. Eisma, Capturing small-scale surface temperature variation across diverse urban land uses with a small unmanned aerial vehicle, Remote Sens. 15 (2023) 2042, doi:10.3390/rs15082042.
[12] E. Alvarez-Vanhard, T. Corpetti, T. Houet, UAV & satellite synergies for optical remote sensing applications: a literature review, Remote Sens. Technol. 3 (2021) 100019, doi:10.1016/j.srs.2021.100019.
[13] J. Naughton, W. McDonald, Evaluating the variability of urban land surface temperatures using drone observations, Remote Sens. 11 (2019) 1722, doi:10.3390/rs11141722.
[14] K. Fabri, V. Constanzo, Drone-assisted infrared thermography for calibration of outdoor microclimate simulation models, Sustain. Cities Soc. 52 (2020) 101855, doi:10.1016/j.scs.2019.101855.
[15] S. Dimitrov, A. Popov, M. Iliev, An application of the LCZ approach in surface urban heat island mapping in Sofia, Bulgaria, Atmosphere 12 (2021) 1370, doi:10.3390/atmos12111370.
[16] Y. Cho, C. Yoon, M.J. Lee, Comparative analysis of urban heat island cooling strategies according to spatial and temporal conditions using Unmanned Aerial Vehicles (UAV), Observation. Appl. Sci. 13 (2023) 10052, doi:10.3390/app131810052.
[17] A. Kantzioura, P. Kosmopoulos, S. Zoras, Urban surface temperature and microclimate measurements in Thessaloniki, Energ. Build. 44 (2012) 63–72, doi:10.1016/j.enbuild.2011.10.019.
[18] Z. Wu, Y. Zhang, Water bodies' cooling effects on urban land daytime surface temperature: ecosystem service reducing heat island effect, Sustainability 11 (2019) 787, doi:10.3390/su11030787.
[19] D. Maroni, G.T. Cardoso, A. Neckel, L.S. Maculan, M.L.S. Olivira, E.T. Bodah, B.W. Bodah, M. Santosh, Land surface temperature and vegetation index as a proxy to microclimate, J. Environ. Chem. Eng. 9 (2021) 105796, doi:10.1016/j.jece.2021.105796.
[20] P. Pereira, M. Kalinauskas, V. Pinto, E. Baltranaite, D. Barcelo, W. Zhao, M. Inacio, A simple method to map pollination ecosystem services potential in urban lawns, MethodsX (2024), doi:10.1016/j.mex.2024.102943.
[21] Y. Liu, S. Liu, J. Wang, X. Zhu, Y. Zhang, X. Liu, Variation in soil respiration under the tree canopy in a temperate mixed forest, central China, under different soil water conditions, Ecol. Res. 29 (2014) 133–142, doi:10.1007/s11284-013-1110-5.
[22] M. Guo, H. Zhang, Y. Huang, Z. Xie, L. Wu, J. Zhang, Shadow removal method for high-resolution aerial remote sensing images based on region group matching, Expert Syst. Appl. 225 (2024) 124739, doi:10.1016/j.eswa.2024.124739.
[23] A.S. Milas, K. Arend, C. Mayer, M.A. Simonson, S. Mackey, Different colours of shadows: classification of UAV images, Int. J. Remote Sens. 31 (2017) 3084–3100, doi:10.1080/01431161.2016.1274449.
[24] E. Barbierato, I. Bernetti, I. Capecchi, C. Saragosa, Quantifying the impact of trees on land surface temperature: a downscaling algorithm at city-scale, Eur. J. Remote Sens. 52 (2019) 74–83, doi:10.1080/22797254.2019.1646104.
[25] Y. Park, J.M. Guldmann, D. Liu, Impacts of tree and building shades on the urban heat island: combining remote sensing, 3D digital city and spatial regression approaches, Comput. Environ. Urban Syst. 88 (2021) 101655, doi:10.1016/j.compenvurbsys.2021.101655.
[26] B. Song, K. Park, Verification of accuracy of Unmanned Aerial Vehicle (UAV) land surface temperature images using in-situ data, Remote Sens. 12 (2019) 288, doi:10.3390/rs12020288.
[27] D. Kim, J. Yu, J. Yoon, S. Jeon, S. Son, Comparison of accuracy of surface temperature images from unmanned aerial vehicle and satellite for precise thermal environment monitoring of urban parks using in situ data, Remote Sens. 13 (2021) 1977, doi:10.3390/rs13101977.
[28] https://www.mdpi.com/2072-4292/14/13/3179
[29] B. Augusto, P. Roebling, S. Rafael, J. Ferreira, A. Ascenso, C. Bodilis, Short and medium- to long-term impacts of nature-based solutions on urban heat, Sustain. Cities Soc. 57 (2020) 102122, doi:10.1016/j.scs.2020.102122.
[30] Z. Zheng, L. Zhao, K.W. Oleson, Large model structural uncertainty in global projections of urban heat waves, Nat. Comm. 12 (2021) 3736, doi:10.1038/s41467-021-24113-9.